

SIMULATE-4 MULTIGROUP NODAL CODE WITH MICROSCOPIC DEPLETION MODEL

Tamer Bahadir

Studsvik Scandpower, Inc.
1087 Beacon St. Suite 301, Newton, MA 02459, USA
tamer.bahadir@studsvikscandpower.com

Sten-Örjan Lindahl

Studsvik Scandpower AB
Hantverkargatan 2A, SE-72212 Västerås, Sweden
sten-orjan.Lindahl@studsvik.se

Scott P. Palmtag

Studsvik Scandpower, Inc.
504 Shoup Ave, Suite 201, Idaho Falls, ID 83402, USA
scott.palmtag@studsvikscandpower.com

ABSTRACT

SIMULATE-4 is a three-dimensional multigroup analytical nodal code with microscopic depletion capability. It has been developed employing “first principal models” thus avoiding ad-hoc approximations. The multigroup diffusion equations or, optionally, the simplified P_3 equations are solved. Cross sections are described by a hybrid microscopic-macroscopic model that includes approximately 50 heavy nuclides and fission products. Heterogeneities in the axial direction of an assembly are treated systematically. Radially, the assembly is divided into heterogeneous submeshes, thereby overcoming the shortcomings of spatially-averaged assembly cross sections and discontinuity factors generated with zero net-current boundary conditions. Numerical tests against higher order transport methods and critical experiments show substantial improvements compared to results of existing nodal models.

KEYWORDS: SIMULATE-4, Nodal, SP_3 , Homogenization, Microscopic Depletion

1. INTRODUCTION

Studsvik’s nodal code SIMULATE-3 [1] has been in use for LWR reactor analysis for nearly 20 years. Due to limitations in memory and computer speed when it was developed, the two-group polynomial method with macroscopic depletion was chosen. The model has proven accurate for typical LWR applications. Today’s increasingly aggressive designs with MOX fuel, part-length fuel rods, extended cycles, and complex operation strategies require more sophisticated reactor physics tools. To meet these concerns, Studsvik has developed a next generation nodal code, SIMULATE-4.

SIMULATE-4 neutronic models are based on ‘first principle models’ and avoid using ad-hoc approximations (such as spectral history corrections). The basis of the new development is 1) the detailed tracking of all important nuclides and their representation with a microscopic depletion model, and 2) the use of multigroup simplified P_3 (SP_3) equations [2,3] or, optionally, diffusion equations. Any number of groups may be used, provided they are a subset of the groups used in the cross-section generator CASMO-4 [4].

The model for solving the three-dimensional multigroup diffusion equation with node-wise constant cross sections is described in Section 2. Should the node be materially heterogeneous in the axial direction, a heterogeneous axial model (Section 3) is used to compute homogenized cross sections and axial discontinuity factors to compensate for these heterogeneities. CASMO-4 has generated assembly-averaged cross sections assuming zero net-currents. In Section 4, a method is presented to adjust cross sections and discontinuity factors to account for flux and material distributions within each node. Also, the inclusion of P_3 transport effects into the global solution is described. The hybrid macroscopic/microscopic cross section model and the tracking of all important nuclides are elaborated in Section 5. Finally, in Section 6, results from numerical testing of SIMULATE-4 are presented.

2. 3D MULTIGROUP SOLVER

The global 3D solver is based on node-wise uniform cross sections. Cross section variations inside the node are handled by axial homogenization model and radial submesh cross section models. The 3D solver runs in tandem with these two models: in each power/void iteration cross sections are re-homogenized and discontinuity factors are adjusted. Also, P_3 effects are built into these updated parameters.

The global model solves the three-dimensional multigroup diffusion equation by the Analytic Nodal Method [5,6]. The 3D diffusion equations are integrated over the transverse directions to give a coupled set of 1D equations. The transverse leakage is approximated by a quadratic fit of the known average out-leakages of three adjoining nodes. The one-dimensional multigroup equation is converted into G ‘one-group’ equations by a transformation employing the eigenvectors of the buckling matrix B^2 . The one-group equation is readily solved, leading to an expression relating the side flux gradient to the side average flux, the node average flux, and the spatial expansion coefficients of the transverse leakage.

By requiring current and flux continuity (or known discontinuity) between two nodes, the net-current as a function of the average fluxes in nodes n and m becomes, after some manipulation, in multigroup formulation

$$\bar{J}_{nm} = (d_n^{-1} + d_m^{-1})^{-1} \cdot (S_n \bar{\phi}_n - S_m \bar{\phi}_m) \quad (1)$$

Here, the d and S matrices are functions of the eigenvalues and eigenvectors of the buckling matrix and of the discontinuity factors. In addition, d depends on the diffusion coefficients and S on the expansion coefficients of the transverse leakage. Substitution of Eq. 1 into the node balance relation

$$\sum_{m=1}^6 \frac{1}{h_{nm}} J_{nm} + \hat{\Sigma}_r \bar{\phi}_n - \hat{\Sigma}_s \bar{\phi}_n - \frac{1}{k} \chi \nu \hat{\Sigma}_f \bar{\phi}_n = 0 \quad (2)$$

yields an equation that contains node average flux as the only unknown. It should be noted, however, that the coefficients of the equation are dependent on the flux solution itself through the S coefficients.

The resultant equations are solved in either of two ways: the one-layer “direct” method based on Chebyshev iteration or two-layers “fission source” iteration in which the outer (source) iteration is accelerated by Wielandt eigenvalue shift and the inner (flux) iteration solved by Cyclic Chebyshev Semi-Iteration.

3. AXIAL HOMOGENIZATION

The purpose of the axial homogenization model is to compute, per node, average cross sections and axial discontinuity factors for an assembly where axial material boundaries do not follow node boundaries. Material discontinuities appear because of:

- Enrichment/burnable absorber zoning
- Spacers
- Control rod tips and control rod absorber zoning
- Assemblies of different heights

Each assembly is axially divided into ‘subnodes’ that follow calculational node boundaries plus material boundaries such that subnodes are always materially uniform. The subnode boundaries can be different in each assembly and are allowed to change during control rod movements.

For each of the assemblies, a separate multigroup one-dimensional diffusion equation is solved in the axial direction over the subnode regions. The influence of neighbouring assemblies is handled by converting the radial leakage, known from the global 3D solution, to an equivalent absorption cross section.

To solve the one-dimensional diffusion equation, the method of section 2, reduced to one dimension, is used. The fission source iteration method is applied, whereby the inner flux equations are solved by direct inversion of a block tri-diagonal system.

Finally, the following is computed:

- Flux weights per subnode and group (to be used to compute node average cross sections)
- Axial discontinuity factors to be used in 3D solver with uniform calculational boundaries

4. RADIAL SUBMESH MODEL

The radial submesh model divides the core into a set of two-dimensional radial slices where each fuel assembly is divided into $N \times N$ rectangular submeshes (Typically, $N=5$).

When subdividing the assembly (or, optionally, PWR quarter-assembly) the submeshes follow pin cell boundaries as defined by the cross section generator. For a BWR, the outer submesh layer is made up of the water gap. For a PWR, the outer layer thickness is chosen to capture intra-assembly mismatch effects.

For each submesh s and group g CASMO-4 generates cross sections, Σ_{gs}^0 , and discontinuity factors, f_{gs} , assuming zero net-currents as assembly boundary condition. The cross sections actually used are modified as

$$\Sigma_{gs} = \Sigma_{gs}^0 + \Delta\Sigma_{gs} \quad (3)$$

The second term, $\Delta\Sigma_{gs}$, gives the change due to differences in burnup, fuel temperature and xenon in the submesh in real life as compared to the idealized conditions prevailing during cross section generation. The $\Delta\Sigma_{gs}$ term for absorption also accounts for the leakage in the z direction (known from the 3D global solver) by converting the axial leakage to an equivalent absorption cross section.

Each 2D submesh problem is solved using either the multigroup diffusion theory or the multigroup SP₃ equations.

The submesh calculations are performed in two steps.

Step 1 - Full 2D calculation. The diffusion or SP₃ transport equation is solved one 2D slice at a time. Once the submesh flux solution is available, homogenized assembly cross sections and discontinuity factors, Σ_g^{2D} , and f_g^{2D} , are computed for each node (i.e., averaged over N×N submeshes). The assembly discontinuity factor is evaluated with a method, which is compatible with the solution method used for the global 3D solution as described in section 2.

Step 2 – Single-Assembly (SA) calculation. For each assembly the diffusion or SP₃ transport equation is solved with zero-net currents as boundary conditions. The submesh non-corrected cross section, Σ_{gs}^0 , and the discontinuity factor, f_{gs} , are employed. Based on the resulting neutron flux, homogenized assembly cross sections, Σ_g^{SA} , and side average discontinuity factors, f_g^{SA} , are computed.

A correction to the conventional node average cross sections and discontinuity factors can now be made

$$\left. \begin{aligned} \Sigma_g^{3D} &= \Sigma_g^{CASMO} + \Sigma_g^{2D} - \Sigma_g^{SA} \\ f_g^{3D} &= f_g^{CASMO} + f_g^{2D} - f_g^{SA} \end{aligned} \right\} \quad (4)$$

Note, that if conditions of the single-assembly calculation are exactly equal to those prevailing in the cross section generator, Σ_g^{CASMO} and Σ_g^{SA} will be identical and $\Sigma_g^{3D} = \Sigma_g^{2D}$. However, conditions may not be identical since the node may be axially heterogeneous, or the submesh cross sections and the node average cross section may have different dependencies.

Conventionally, core simulators are based on assembly average cross sections generated by employing zero net-current boundary conditions. As a consequence, cross sections and discontinuity factors are computed using a stereotype flux distribution, not the real one. Obviously, the submesh model overcomes this shortcoming and accounts for:

- Assembly internal cross section variations
- Weighting with a correct flux when computing node averaged cross sections
- Intra-assembly mismatch effects (spatial and spectral)
- Transport effects (through the SP₃ model and submesh discontinuity factors)
- Gap width mismatch effects (if BWR)

Because of the way the submesh model computes discontinuity factors, the global solver reproduces the submesh results exactly if calculations are made on a 2D core (and, hence there is no axial leakage). The reason SIMULATE-4 involves a global solver at all, and does not rely entirely on the submesh model (in 3D), is that the submesh calculations are less accurate for large meshes. Hence, since we want to keep a large axial mesh, the global model is needed to stitch the 2D submesh slices together.

Since most of the computing time of SIMULATE-4 neutronics is spent on the submesh calculations, it is important that the corresponding algorithm is fast and accurate. A description of the solution method now follows.

The simplified P₃ equations for group g are [7]

$$-D_{1g} \nabla^2 \Phi_{0g} + \Sigma_{r1g} \Phi_{0g} = Q_g + 2\Sigma_{r1g} \phi_{2g} \quad (5)$$

$$-D_{3g} \nabla^2 \phi_{2g} + \frac{5}{3} \Sigma_{totg} \phi_{2g} = \frac{2}{3} (\Sigma_{r1g} \phi_{0g} - Q_g) \quad (6)$$

where ϕ_{0g} is the scalar flux and

$$\Phi_{0g} = \phi_{0g} + 2\phi_{2g} \quad (7)$$

$$Q_g = \frac{1}{k_{eff}} \chi_g \sum_{g'=1}^G \nu \Sigma_{fg'} \phi_{0g'} + \sum_{\substack{g'=1 \\ g' \neq g}}^G \Sigma_{sgg'} \phi_{0g'} \quad (8)$$

$$D_{1g} = \frac{1}{3\Sigma_r} \quad (9)$$

$$D_{3g} = \frac{3}{7\Sigma_{tot}} \quad (10)$$

Obviously, the equation for Φ_0 may be evaluated with the same algorithm as used for ϕ_2 , but with a different source term. The two equations are solved iteratively, first solving Eq. 5 using an estimate of ϕ_2 , then solving Eq. 6.

Equations 5 and 6 can be summarized as

$$-D \frac{\partial^2 \phi}{\partial x'^2} - D \frac{\partial^2 \phi}{\partial y'^2} + \Sigma_r \phi = \tilde{Q}(x', y') \quad (11)$$

Equation 11 is to be solved for a rectangular node of size $h_x \times h_y$. It will be assumed that the source term is a quadratic polynomial in x and y . By converting to dimensionless coordinates, Eq. 11 becomes

$$-\frac{\partial^2 \phi}{\partial x^2} - \frac{h_x^2}{h_y^2} \frac{\partial^2 \phi}{\partial y^2} + \kappa_x^2 \phi = q_0 + \sum_{l=1}^2 q_{xl} P_l(x) + \frac{h_x^2}{h_y^2} \sum_{l=1}^2 q_{yl} P_l(y) \quad (12)$$

where P_l are the Legendre polynomials and where

$$\kappa_x^2 = \frac{h_x^2 \Sigma_r}{4 D} \quad (13)$$

As an approximate solution to Eq. 12 we shall assume

$$\phi(x, y) = \sum_{i=1}^4 K_i v_i(x, y) + c_0 + \sum_{l=1}^2 (c_{xl} P_l(x) + c_{yl} P_l(y)) \quad (14)$$

$$v_1 = e^{-\kappa_x x}, \quad v_2 = e^{+\kappa_x x}, \quad v_3 = e^{-\kappa_y y}, \quad v_4 = e^{+\kappa_y y} \quad (15)$$

The four unknown expansion coefficients K_i of Eq. 14 are found from four node boundary conditions (node average side fluxes). The c_i coefficients are evaluated by substituting Eq. 14 into Eq. 12 and matching terms.

It may be shown, after considerable algebra, that the side average flux gradients are related to the side average flux, node average flux, and source expansion coefficients as

$$\left. \begin{aligned} + \frac{\partial \phi}{\partial x} \Big|_{+x} &= t_x (\phi_{+x} - \bar{\phi} + \xi_x g_x - \eta_{x1} q_{x1} - \eta_{x2} q_{x2}) \\ - \frac{\partial \phi}{\partial x} \Big|_{-x} &= t_x (\phi_{-x} - \bar{\phi} + \xi_x g_x + \eta_{x1} q_{x1} - \eta_{x2} q_{x2}) \end{aligned} \right\} \quad (16)$$

and analogously for the y direction. Here we have defined:

$$g_x = \left. \frac{\partial \phi}{\partial x} \right|_{+x} - \left. \frac{\partial \phi}{\partial x} \right|_{-x} \quad (17)$$

$$\left. \begin{aligned} \Lambda_x &= \frac{\tanh \kappa_x}{\kappa_x} \\ t_x &= \frac{1}{\Lambda_x} = 1 + \frac{1}{3} \kappa_x^2 - \frac{1}{45} \kappa_x^4 + \dots \\ \xi_x &= \frac{\Lambda_x}{2} - \frac{1 - \Lambda_x}{2 \kappa_x^2 \Lambda_x} = \frac{1}{3} \left(1 + \frac{7}{15} \kappa_x^2 + \frac{11}{525} \kappa_x^4 + \dots \right)^{-1} \\ \eta_{x1} &= \frac{1 - \Lambda_x}{\kappa_x^2} = \frac{1}{3} \left(1 + \frac{2}{5} \kappa_x^2 - \frac{1}{525} \kappa_x^4 + \dots \right)^{-1} \\ \eta_{x2} &= \frac{1}{\kappa_x^2} - 3 \frac{1 - \Lambda_x}{\kappa_x^4 \Lambda_x} = \frac{1}{15} \left(1 + \frac{2}{21} \kappa_x^2 - \frac{1}{2205} \kappa_x^4 + \dots \right)^{-1} \end{aligned} \right\} \quad (18)$$

Obviously, iteration is needed when employing Equations 16 since the gradients depend on the gradients themselves through the g_x term.

The source term of Eq. 11 depends on the flux. Therefore, in order to compute the source expansion moments of Eq. 12 we need to know the flux expansion moments. These are found by projecting the flux of Eq. 14 onto the first three Legendre polynomials.

Equation 16 can be simplified by introduction of the auxiliary variables ψ , ε , μ_x and μ_y :

$$\psi = \bar{\phi} - \frac{1}{2} \xi_y g_y - \frac{1}{2} \xi_x g_x + \frac{1}{2} \eta_{y2} q_{y2} + \frac{1}{2} \eta_{x2} q_{x2} \quad (19)$$

$$\varepsilon = \frac{1}{2} \xi_y g_y - \frac{1}{2} \xi_x g_x - \frac{1}{2} \eta_{y2} q_{y2} + \frac{1}{2} \eta_{x2} q_{x2} \quad (20)$$

$$\left. \begin{aligned} \mu_x &= \eta_{x1} q_{x1} \\ \mu_y &= \eta_{y1} q_{y1} \end{aligned} \right\} \quad (21)$$

If the in-leakage is nearly the same in the x and y directions and if the source term is almost symmetric in x and in y , then ε , μ_x , and μ_y will be very small compared to ψ . This is the reason why the auxiliary variable ψ is introduced.

Equation 16 can now be written

$$\left. \begin{aligned} + \left. \frac{\partial \phi}{\partial x} \right|_{+x} &= t_x (\phi_{+x} - \psi - \varepsilon - \mu_x) \\ - \left. \frac{\partial \phi}{\partial x} \right|_{-x} &= t_x (\phi_{-x} - \psi - \varepsilon + \mu_x) \\ + \left. \frac{\partial \phi}{\partial y} \right|_{+y} &= t_y (\phi_{+y} - \psi + \varepsilon - \mu_y) \\ - \left. \frac{\partial \phi}{\partial y} \right|_{-y} &= t_y (\phi_{-y} - \psi + \varepsilon + \mu_y) \end{aligned} \right\} \quad (22)$$

The sum $\psi + \varepsilon$ ($\psi - \varepsilon$) acts as a fictitious midpoint flux for the x (y) direction of a node.

As in Section 2, the gradient expressions are used to set up an expression for the net leakage between two nodes (compare Eq. 1). Furthermore, substitution into the node balance equation (Eq. 2) gives a finite difference like equation for ψ

$$a_n \psi_n - \sum_{m=1}^6 C_{nm} \psi_m = Q_n + \Delta Q_n(\varepsilon, \mu_x, \mu_y) \quad (23)$$

Here, Q_n represents the node average value of the right hand side of Eq. 11. The ΔQ_n term represents the collection of all terms dependent on ε , μ_x , and μ_y .

The SP₃ (or diffusion) equation is solved by the source iteration technique. The $\bar{\phi}$, q_i , ε , μ_x , μ_y , and ΔQ_n are updated in the outer iteration loop.

5. MICROSCOPIC DEPLETION MODEL

In SIMULATE-4 the traditional macroscopic depletion model is replaced by a hybrid macro/micro model in which the node-average cross sections at the given actual condition are estimated as:

$$\Sigma_{\alpha}^{actual} = \Sigma_{\alpha}^{SA}(E, \rho_h, \rho, \dots) + \sum_i \sigma_{\alpha i}(E, \rho_h, \rho, \dots)(N_i^{actual} - N_i^{SA}(E, \rho_h, \dots)) \quad (24)$$

The Σ_{α} represents Σ_a , Σ_f , and $\nu\Sigma_f$, and the summation is over selected nuclides. The second term in Eq. 24 provides a correction to the single-assembly macroscopic cross sections (Σ_{α}^{SA}) to make up for the fact that real life operation (represented by number density N^{actual}) differs from the idealized condition of the single-assembly CASMO-4 evaluation (represented by N^{SA}).

Approximately 50 isotopes (17 actinides, 30 fission products, Gd/B¹⁰ as burnable absorber) have been chosen according to their importance on reactivity during normal operation, depletion, transients and shutdowns (with possible long outages).

Both the macroscopic and microscopic multigroup cross sections appearing in Eq. 24 are functionalized in two- and three-dimensional tables versus all important instantaneous effects (e.g., coolant density, control rod, fuel temperature, etc.) and historical effects (e.g., burnup, coolant density history, and control rod history).

The reference single-assembly number densities are functions of burnup and historical effects. The N^{SA} are not taken directly from CASMO-4 but calculated in the linking code by solving the SIMULATE-4 isotope chains using the single-assembly fluxes and microscopic cross sections. Hence, N^{SA} and N^{actual} are computed in consistent manners.

Due to its large spatial self-shielding, the Gd isotopes require a special treatment. The chain of gadolinium isotopes (Gd^{155} - Gd^{156} - Gd^{157}) has been replaced by an effective Gd isotope [8]. The

number density and microscopic absorption cross section for the effective Gd isotope are defined as:

$$N_{Gd^{Eff}} = 3N_{Gd^{155}} + 2N_{Gd^{156}} + N_{Gd^{157}} \quad (25)$$

$$\sigma_{Gd^{Eff}} = \frac{N_{Gd^{155}}\sigma_{Gd^{155}} + N_{Gd^{156}}\sigma_{Gd^{156}} + N_{Gd^{157}}\sigma_{Gd^{157}}}{N_{Gd^{Eff}}} \quad (26)$$

The microscopic absorber cross section of Gd^{Eff} is given as a function of the number density of Gd^{Eff} itself.

The actual number densities appearing in Eq. 24 are tracked for each node using the node average fluxes available from the multigroup nodal solver. The burnup chain calculations in SIMULATE-4 are carried out in two steps according to the predictor/corrector technique. The linearized chain equations are solved by direct integration.

6. NUMERICAL TESTING

6.1 Microscopic Depletion Model Verification: Single-Assembly/Mini-core

The microscopic depletion model in SIMULATE-4 is verified against a single-assembly 2D CASMO-4 calculation. The traditional macroscopic depletion model is also compared with the microscopic model. Figure 1 presents the eigenvalue error for a typical BWR assembly with Gd (2.8 wt% U235 enrichment with eight GdO₂ pins of 4 wt%) during an unrodded-rodded-unrodded depletion sequence. The deficiency of the macroscopic depletion model following the pulling of the control rod after 20 GWD/Mt has been significantly alleviated with the micro

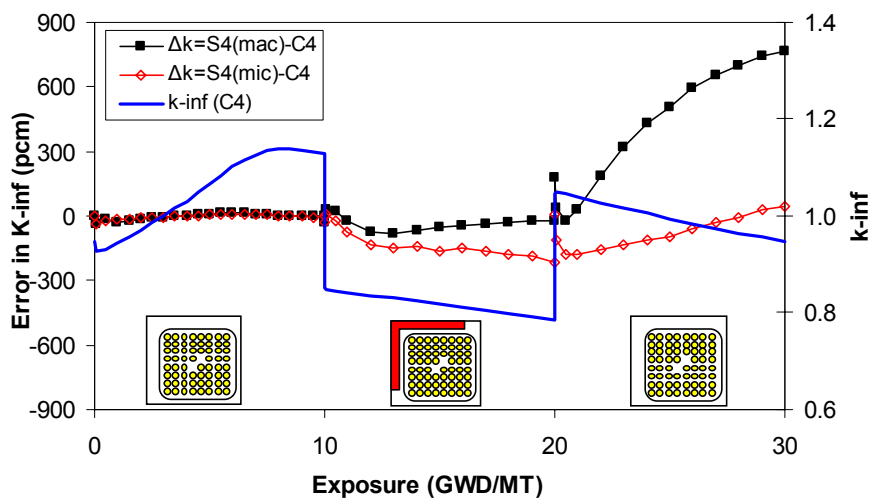


Figure 1. Reactivity error for a BWR single-assembly depletion: unrodded-rodded-unrodded

depletion model. Figure 2 presents the error in tracking the number densities for some actinides at 25 GWD/Mt with the microscopic and macroscopic cross section models, respectively. The isotopic number densities for the macroscopic cross section model are found by table look-up interpolation, similar to that used in evaluating the macroscopic cross sections, for the given exposure and control rod history. The isotopic number densities tracked with the microscopic depletion model match the reference number densities including end chain isotopes. Although some of these isotopes may not be crucial for reactivity, their accurate predictions are important for safeguard reporting.

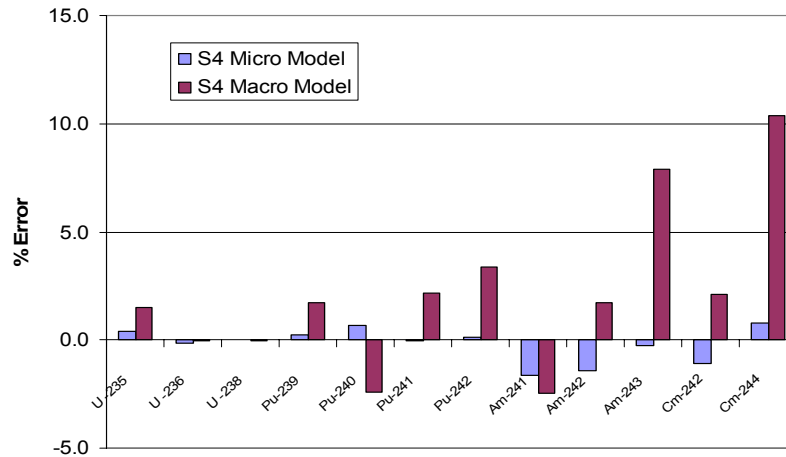


Figure 2. Error in actinide number densities at 25 GWD/Mt for a single-assembly unrodded-rodded-unrodded depletion

In the next case, the single-assembly testing is extended to mini-core depletion. A 3×3 arrangement of BWR 8×8 assemblies is built of three fuel types with average enrichments of 1.3 wt%, 2.5 wt% and 3.8 wt%, respectively. The last two assembly designs also include Gd pins. The enrichment splits are typical for first cycle operation of a BWR. The core layout, with the location of the control rod marked, is shown in Figure 3. The core is depleted with the control rod inserted until 8 GWD/Mt where the control rod is pulled for the remainder of the depletion.

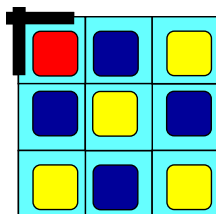


Figure 3. BWR mini-core of 3×3 assemblies

The reference solution is obtained from CASMO-4E [9] with 16 energy groups and 3×3 assemblies. All SIMULATE-4 calculations are performed with the radial submesh homogenization model. Comparisons between CASMO-4E and SIMULATE-4 are shown in Figure 4. The microscopic depletion results show improvements both in eigenvalue and in power distribution. Adding more energy groups for this 2D BWR depletion problem has very little impact on results.

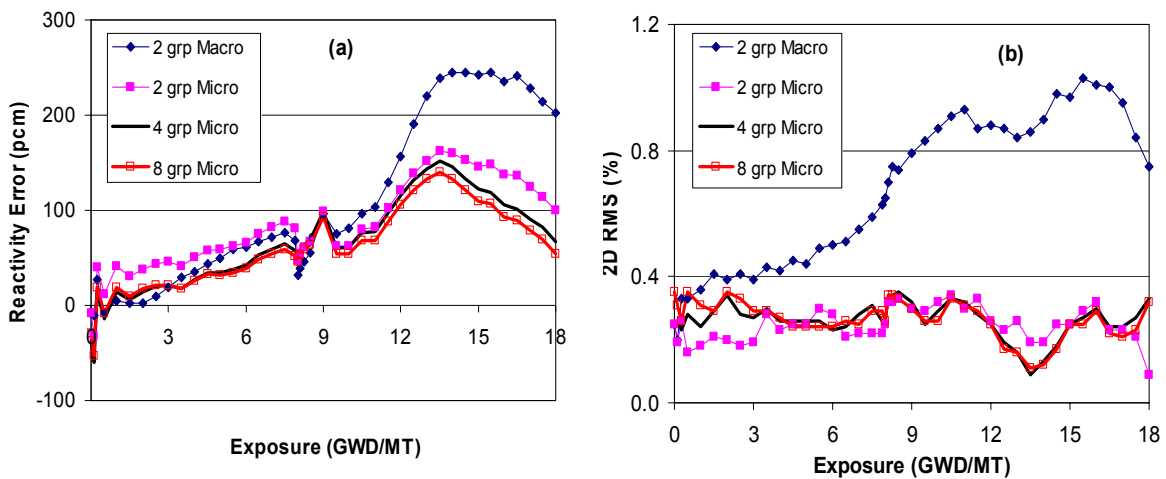



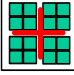

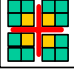
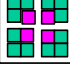
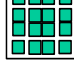

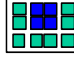

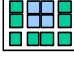
Figure 4. BWR 3x3 mini-core depletion: error in (a) reactivity and (b) assembly power predictions

6.2 Radial Submesh Model Verification: KRITZ-4 Critical Experiments

The radial submesh homogenization model is verified by evaluation of a set of boiling water reactor cores of the KRITZ facility [10]. The KRITZ critical experiments represent realistic core configurations with an arrangement of 4x4 BWR 8x8 assemblies. Criticality has been achieved by adjusting the boron concentration in the coolant. Core configurations differ with respect to Gd content, presence of control rod, and the location of wide/narrow water gap. A series of SIMULATE-4 calculations at the measured critical boron concentrations are performed with and without the submesh homogenization model in 2, 4, 8 and 16 energy groups. Results are summarized in Table I. CASMO-4E full core model results, generated in 16 energy groups, are also shown in this table. Cores 2:1 and 3:1 are especially interesting with respect to homogenization. Both cores have been constructed using the same fuel layout but with different gap orientation. Core 2:1 has the wide water gaps at the center while core 3:1 has the narrow water gaps at the configuration center. With conventional homogenization of water gaps and fuel, the two cores look identical. Consequently, the predicted critical boron concentrations would be the same for the two cores, which is inconsistent with the measured data [11]. As can be seen from Table I, the SIMULATE-4 eigenvalues without submesh homogenization differ by as much as 600 pcm. Employing the submesh model, the difference in critical eigenvalues is reduced to 80 pcm in two-group calculations. The same trend, improvement with the submesh model, can be seen for all core configurations.

The two-group method is not capable of capturing the high leakage of these mini-cores. The improvement in predicting the critical eigenvalue is significant with more energy groups. The average eigenvalue is reduced to 0.9995 with a standard deviation of 85 pcm for 8 and 16 energy groups.

Table I. Eigenvalue Predictions with SIMULATE-4 for KRITZ-4 Critical Cores

CORE		SIMULATE-4		SIMULATE-4 Submesh Model				CASMO-4
		2 grp	16 grp	2 grp	4grp	8 grp	16 grp	
	2:1	0.99955	0.99708	1.00390	1.00161	1.00070	1.00067	0.99950
	2:2	0.99719	0.99310	1.00503	1.00092	0.99943	0.99940	0.99980
	2:3	0.99823	0.99559	1.00382	1.00141	1.00037	1.00034	0.99967
	2:4	0.99509	0.99031	1.00483	1.00011	0.99858	0.99854	0.99954
	2:5	0.99493	0.99092	1.00470	1.00122	0.99981	0.99978	0.99952
	3:1	1.00523	1.00187	1.00459	1.00160	1.00059	1.00058	1.00014
	3:2	1.00904	1.00504	1.00367	1.00032	0.99888	0.99885	1.00017
	3:3	1.00815	1.00457	1.00291	0.99993	0.99862	0.99859	0.99923
	3:4	1.00879	1.00558	1.00410	1.00147	1.00028	1.00026	1.00053
	3:5	1.00823	1.00464	1.00287	0.99990	0.99866	0.99864	1.00039
AVE		1.00244	0.99887	1.00404	1.00085	0.99959	0.99957	0.99985
STD (pcm)		598	616	76	71	86	87	43

6.3 Multigroup Solver/SP₃ Testing: ¼ MOX Core

A simple PWR ¼ core problem with MOX fuel is evaluated. The core contains 148 fuel assemblies of 17×17 pin design. The fresh UO₂ assemblies comprise pins of 2.1 % and 4.1 % enrichment (with 0 and 20 burnable absorber pins, respectively). The MOX fuel assemblies contain three different pin enrichments (4.0 %, 6.0 % and 8.0 % total plutonium). A reference solution is obtained from a CASMO-4E calculation performed in 16 energy groups. A set of SIMULATE-4 calculations with and without the SP₃ model is performed in 2, 4, 8 and 16 energy groups. Figure 5 presents the core configuration and shows the error in assembly powers for 16-group solutions. The eigenvalue and assembly power results are listed in Table II. The accuracy of the nodal model improves with more energy groups. Provided that there are a sufficiently large number of energy groups (8 or more), the SIMULATE-4 predictions are further improved with the inclusion of the SP₃ model.

Finally, a set of core depletion calculations are performed employing the macroscopic and microscopic models, respectively, in 2, 4 and 8 energy groups. SIMULATE-4 solutions are compared to the CASMO-4E solution. Figure 6 presents the error in eigenvalue and the RMS error in assembly power for the various models. Both the eigenvalue and the power predictions are improved with the microscopic depletion model coupled with more energy groups.

Table II. PWR MOX Core: Results Summary

MODEL	Number of Energy Groups	Delta K (pcm)	Assembly Power Max Error (%)	Assembly Power RMS (%)
Submesh	2	175	4.30	1.93
	4	107	2.50	1.37
	8	34	2.40	1.13
	16	-21	2.00	0.95
Submesh+SP ₃	2	198	5.20	2.15
	4	124	2.90	1.33
	8	54	1.70	0.91
	16	7	1.10	0.65

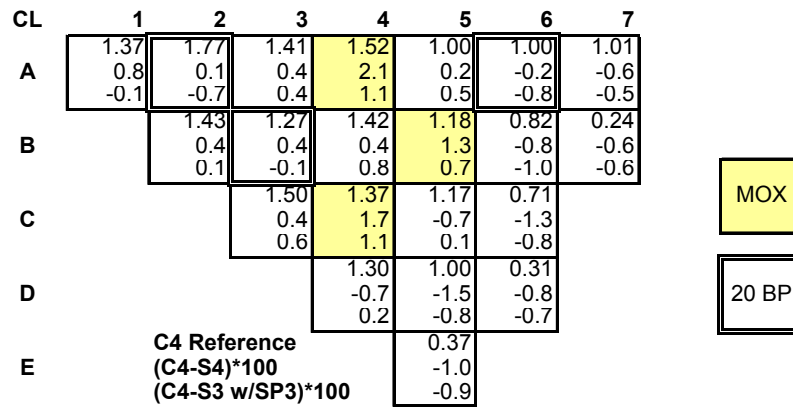


Figure 5. PWR MOX core: error in assembly power distributions with 16 group solution

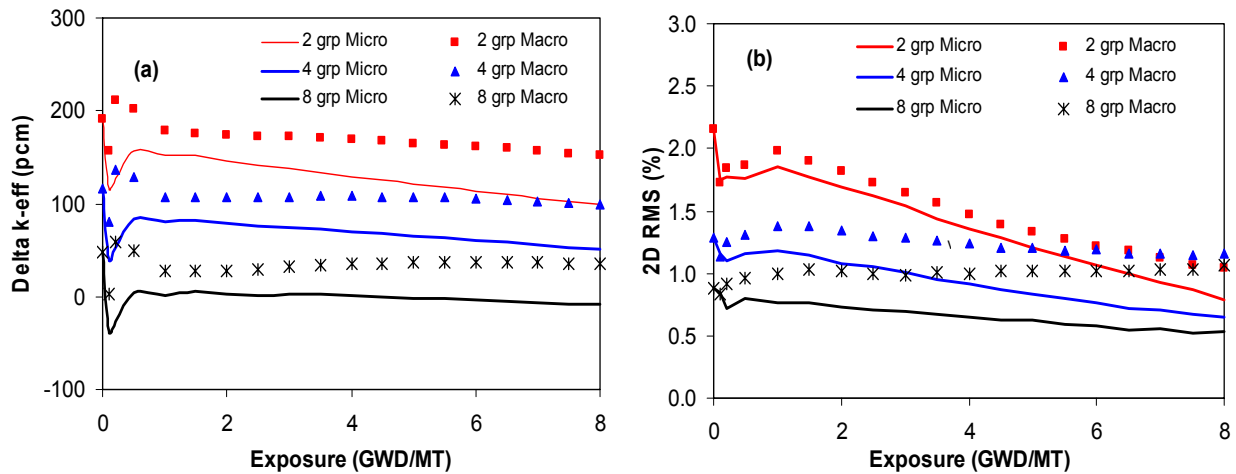


Figure 6. PWR MOX core depletion: error in (a) reactivity and (b) assembly power predictions

7. CONCLUSIONS

SIMULATE-4 is a three-dimensional multigroup analytical nodal code with microscopic depletion capability. It has been developed employing “first principal methods” avoiding ad-hoc approximations. In this paper, the neutronic models are presented in detail. Various models in the code are validated for test problems where SIMULATE-4 results are compared to higher order reference solutions or to criticality experiments. Numerical studies show that more than two-energy groups are needed for accurate modelling of cores with high leakage or with large spectral mismatch between the assemblies as in the case of MOX. Assembly submesh homogenization combined with the SP₃ method improves results where transport and homogenization effects are important. Deficiencies of the traditional macroscopic depletion model are removed with the hybrid micro/macro depletion model.

Validation of SIMULATE-4 by core tracking is now underway [12].

REFERENCES

1. K.S. Smith et al., ‘SIMULATE-3 Methodology’, Studsvik/SOA-95/18 (1995).
2. E. Gelbard, “Application of Spherical Harmonics Method to Reactor Problems”, WAPD-BT-20 (Sept.1960).
3. K.S. Smith, “A Multidimensional Nodal Transport Using the Simplified P_L Method”, *Proc. Topl. Mtg. on Reactor Physics and Safety*, Saratoga Springs, NY, USA, p.223 (1986).
4. M. Edenius et al., “CASMO-4, A fuel Assembly Burnup Program, User’s Manual”, Studsvik/SOA-95/1 (1995).
5. K.S. Smith, “An Analytic Nodal Method for Solving the 2-Group, Multi-Dimensional, Static and Transient Neutron Diffusion Equation”, Master’s Thesis, Dep. Nucl. Eng., MIT, Cambridge, MA, USA (1979).
6. D.L. Vogel, Z. J. Weiss, “A General, Multi-Group Formulation of the Analytic Nodal Method”, *Proc. Topical Meeting on Advances in Reactor Physics*, Charleston, SC, USA, March 8-11 (1992).
7. P.S. Brantley, E.W. Larsen, “The Simplified P₃ Approximation”, *Nucl. Sci. Eng.*, **134**, 1-21 (2000).
8. Z. Weiss, “A Consistent Definition of the Number Density of Pseudo-Isotopes”, *Ann. Nucl. Energy*, **17**, No.3, 153-156 (1990).
9. K.S. Smith, J.D.Rhodes, III, “Full-core, 2-D LWR Core Calculations with CASMO-4E,” PHYSOR-2002. Seoul (October, 2002).
10. E. Johnsonn, “Data and Results for KRITZ experiments on Regular H₂O/Fuel Pin Lattices at Temperatures up to 245°C,” Studsvik/NS-90/133, Studsvik (1990).
11. K.S. Smith, “Practical and Efficient Iterative Method for LWR Fuel Assembly Homogenization,” *Trans. Am. Nuc. Soc.*, **71**, 238-241 (1994).
12. S. Yoshida, S. Kosaka, “Real Core Tracking Analyses Using SIMULATE-4,” *Trans. Am. Nuc. Soc.*, **92**, 637-638 (2005).